Biotechnology and Bioengineering

WILEY

BIOTECHNOLOGY AND BIOENGINEERING

ARTICLE OPEN ACCESS

A Method for Optical Quantification of Local Oxygen Limitations in Multiphase Bioreactors

Ryan Rautenbach[1] | Katharina Zörner[1] | Jonas Barczyk[2] | Marko Hoffmann[1] | Ralf Takors[2] | Michael Schlüter[1]

[1]Institute of Multiphase Flows, Hamburg University of Technology, Hamburg, Germany | [2]Institute of Biochemical Engineering, University of Stuttgart, Stuttgart, Germany

Correspondence: Ryan Rautenbach (ryan.rautenbach@tuhh.de) | Michael Schlüter (michael.schlueter@tuhh.de)

Received: 29 April 2026 | **Revised:** 11 June 2026 | **Accepted:** 13 June 2026

Funding: Deutsche Forschungsgemeinschaft, Grant/Award Number: 427899833

Keywords: bioreactors | gas-liquid systems | methylene blue | oxygen limitation | redox chemistry | stirred tank reactors

ABSTRACT

Spatial oxygen limitation is a major source of physiological stress and metabolic, scale-dependent heterogeneity in aerobic bioprocesses. In gas-liquid stirred tank reactors, oxygen availability is governed by hydrodynamics and mass transfer and is therefore inherently non-uniform. Despite its importance, experimentally accessing spatial information on oxygen local supply remains challenging, as most established techniques rely on point-wise sensing or intrusive tracer-based methods. This work presents an optical method for visualizing local oxygen limitation based on the reversible redox chemistry of methylene blue in alkaline glucose solutions. After driving the reactor into a uniformly reduced, colorless state, the spatial reoxidation of the indicator during oxygen aeration is recorded and evaluated pixel-wise. The resulting two-dimensional fields of colorization time provide a spatially continuous indicator of local oxygen supply governed by hydrodynamic transport and gas-liquid mass transfer. Systematic experiments were conducted to assess the influence of glucose and sodium hydroxide concentration on the stability and reproducibility of the redox system, enabling the selection of a robust reaction medium. The method was then applied to a laboratory-scale stirred tank operated at different impeller speeds. The resulting colorization fields reveal characteristic spatial structures associated with oxygen-limiting regions, including insufficiently supplied zones under weak agitation, progressive homogenization with increasing turbulence, and residual transport limitations near reactor walls at high agitation rates. The presented approach requires no local tracer injection and operates under normal aeration conditions, providing qualitative yet physically meaningful insight into oxygen-supply and mixing related heterogeneities. It therefore offers a simple and cost-effective tool for identifying limiting operating points, supporting future scale-transfer studies, and complementing CFD-based analyses of oxygen transport in stirred tank bioreactors.

1 | Introduction

Oxygen availability is a central factor governing the performance, robustness, and scalability of aerobic bioprocesses. Insufficient oxygen supply can induce metabolic shifts, reduce productivity, and promote heterogeneous population responses, particularly in large-scale stirred tank bioreactors. Even under nominally well-mixed conditions, the spatial distribution of dissolved oxygen (DO) is rarely uniform, as it emerges from complex interactions between gas-liquid mass transfer, turbulent transport, bubble dynamics, and reactor geometry (Doran 2013; Shuler and Kargi 2002; Gaugler et al. 2024; Kuschel and Takors 2020).

In stirred tank reactors, hydrodynamic structures such as impeller discharge streams, circulation loops, baffle-induced secondary flows, and near-wall recirculation zones strongly influence how

oxygen is distributed throughout the vessel. Regions in which local oxygen supply is weaker than transport or consumption may act as oxygen-limiting zones, giving rise to spatially heterogeneous exposure histories. Identifying and characterizing such zones is therefore essential for understanding hydrodynamic-biological interactions, designing representative scale-down systems, and validating computational fluid dynamics (CFD) models of gas-liquid mass transfer (Nienow 2014; Zlokarnik 1999; Tatterson 1991; Kadic and Heindel 2014; Rosseburg 2019).

Despite this relevance, experimental access to spatially resolved oxygen information in stirred tanks remains limited. Conventional electrochemical and optical DO probes provide accurate local measurements, but are inherently pointwise and intrusive, offering only sparse spatial coverage within the reactor. While CFD simulations can predict spatial oxygen concentration fields, their validation is constrained by the lack of experimentally accessible, spatially continuous reference data (Van't Riet 1979; Gogate and Pandit 1999; Brooks et al. 1982; Kuschel et al. 2021).

To overcome the limitations of fixed probes, alternative concepts such as flow-following or mobile sensors have been explored. However, these approaches remain restricted in their ability to resolve entire reactor volumes, with most implementations limited to axial measurements. In addition, constraints related to sensor miniaturization, temporal resolution, signal robustness, and performance in multiphase flow environments further limit their applicability in stirred tank reactors (Hofmann et al. 2025; Haringa et al. 2025; Bisgaard et al. 2020; Stine et al. 2020).

As a result, optically accessible, dye-based experiments have become widely used for spatial characterization of mixing and transport phenomena. These methods enable non-intrusive, two-dimensional visualization of hydrodynamically induced heterogeneities that cannot be resolved with conventional probes, and have therefore proven valuable for identifying dead zones, slow-mixing regions, and transport limitations (Hoogendoorn 1967; Nienow 1997; Ascanio et al. 2002, 2015; Fitschen, Hofmann, Wutz et al. 2021).

Several optical approaches for visualizing dissolved oxygen distributions have also been reported, most notably fluorescence- and phosphorescence-based sensing techniques employing ruthenium complexes or related indicator dyes. These methods offer high sensitivity and fast temporal response through oxygen-dependent luminescence quenching. However, they typically rely on laser excitation or pulsed illumination to resolve luminescence lifetimes with sufficient accuracy. Such requirements complicate their application in stirred tank reactors, where long and variable optical path lengths, curved vessel walls, rotating internals, and multiphase flow conditions interfere with both excitation and signal detection. Consequently, these techniques are often confined to specialized experimental setups or simplified geometries rather than fully representative stirred tanks (Wolfbeis 2015; Zhang et al. 2024; PreSens Precision Sensing GmbH 2025; Rüttinger et al. 2018).

Spatially resolved hydrodynamic characterization in transparent stirred tanks has therefore most commonly relied on local mixing time measurements based on optically detectable tracer injections, such as acid-base systems. While these methods are highly effective for analyzing mixing dynamics, the resulting spatial patterns depend strongly on the tracer injection location and its initial transport pathway. Tracers introduced near the impeller emphasize rapid local mixing, whereas injections near the surface or in poorly mixed regions can bias the observed response toward specific circulation structures. Consequently, inferred heterogeneities may reflect the tracer introduction strategy as much as the intrinsic oxygen-supply characteristics of the reactor (Fitschen, Hofmann, Wutz et al. 2021; Ascanio et al. 2002; Hofmann et al. 2024; Weiland et al. 2023).

Compared with these approaches, the methylene-blue method introduced here occupies an intermediate position between point-wise oxygen sensing, tracer-based mixing-time measurements, and specialized luminescence-based oxygen imaging. Unlike fixed DO probes, it provides spatially continuous optical information. Unlike local tracer-injection methods, the observed colorization pattern is not initiated by a local perturbation but by oxygen aeration through the gas phase. Unlike fluorescence- or phosphorescence-based oxygen imaging, it does not require lifetime detection, laser excitation, or specialized optical hardware. The method is therefore not intended to replace quantitative oxygen sensors or laser-based techniques, but to provide a simple projection-based screening tool for identifying operating conditions and reactor regions associated with delayed oxygen supply.

Against this background, there is a clear need for experimentally accessible methods that visualize local oxygen supply directly, without relying on localized tracer injection or advanced optical imaging systems. Such approaches would complement existing techniques by providing spatial information intrinsically linked to gas-liquid mass transfer under realistic multiphase flow operation (Van't Riet 1979; Gogate and Pandit 1999; Wolfbeis 2015; Fitschen, Hofmann, Wutz et al. 2021).

In this work, an optical method based on the reversible redox chemistry of methylene blue is introduced to visualize local oxygen limitation in stirred tank bioreactors. In alkaline glucose solutions, methylene blue reversibly cycles between a colored oxidized form and a colorless reduced form depending on oxygen availability. By driving the reactor into a uniformly reduced state and recording the subsequent spatial reoxidation during oxygen aeration, two-dimensional fields of colorization time are obtained. These fields provide a spatially continuous indicator of local oxygen supply governed by hydrodynamic transport and gas-liquid mass transfer (Anderson et al. 2012; Engerer and Cook 1999; Cook et al. 1994; Piccione et al. 2017).

The objectives of this study are to (i) establish suitable reaction-medium conditions for stable and reproducible operation of the redox indicator system, (ii) demonstrate the application of the method across a range of hydrodynamic operating points in a stirred tank reactor, and (iii) illustrate how local colorization fields can be used to identify oxygen-limiting regions and transport heterogeneities. Overall, this work introduces and evaluates an optical method that provides qualitative yet physically meaningful insight into oxygen-supply heterogeneities, thereby expanding the experimental toolbox available for mixing and transport characterization in gas-liquid reactors.

2 | Background

2.1 | Oxygen Limitation and Mixing Quantifications in Stirred Tank Bioreactors

In gas-liquid stirred tanks, oxygen supply is governed by the combined effects of gas-liquid mass transfer and liquid-phase mixing. Flow structures such as impeller discharge streams, circulation loops, baffle-induced secondary flows, and near-wall recirculation zones determine how dissolved oxygen is transported through the vessel. Consequently, local oxygen availability can remain heterogeneous even when the reactor appears macroscopically well mixed (Nienow 2014; Zlokarnik 1999; Tatterson 1991).

From a bioprocess perspective, such heterogeneities are relevant because cells may experience fluctuating oxygen conditions along their trajectories through the reactor. Identifying regions with delayed or insufficient oxygen supply is therefore important for interpreting scale-dependent process behavior, designing representative scale-down systems and validating CFD-based descriptions of oxygen transport (Shuler and Kargi 2002; Kuschel and Takors 2020; Gaugler et al. 2024).

Established experimental approaches provide only partial access to this information. DO probes offer accurate local measurements but remain spatially sparse, whereas optical tracer-based mixing-time methods provide spatial information on scalar homogenization that can depend on the tracer injection position and initial transport pathway (Hoogendoorn 1967; Ascanio et al. 2002, 2015; Fitschen, Hofmann, Wutz et al. 2021). An approach that visualizes oxygen supply without a localized injection event can therefore complement existing methods by linking the observed spatial response directly to gas-liquid mass transfer and hydrodynamic oxygen transport.

2.2 | Redox Behavior of the Methylene Blue Indicator

The method introduced in this work is based on the reversible redox cycle of methylene blue (MB) as a 1% aqueous solution, which exists in two visually distinct oxidation states. In its oxidized form (MB^+), the dye appears intensely blue, whereas in the reduced leuco form (MBH) the dye is essentially colorless. In alkaline solution containing a reducing sugar such as glucose, the system undergoes continuous cycling between these two states depending on the availability of dissolved oxygen. This behavior forms the basis for using the color transition as an indicator of local oxygen supply (Anderson et al. 2012; Engerer and Cook 1999; Cook et al. 1994).

In strongly alkaline media, glucose (GH) undergoes base-catalyzed activation, forming a transient reducing sugar intermediate. Hydroxide ions facilitate this transformation by abstracting a proton from glucose, thereby generating a highly reactive reducing species derived from the sugar. This activated glucose species exhibits a significantly higher reducing power than the parent glucose molecule. Several studies report that the formation of this reducing intermediate is strongly pH-dependent and is generally regarded as the rate-determining step within the overall reduction pathway (Anderson et al. 2012; Limpanuparb et al. 2017).

Once formed, the activated glucose species reacts with oxidized methylene blue according to:

$$MB^+ + C_6H_{12}O_6 + OH^- \longrightarrow MBH + C_6H_{11}O_6^- + H_2O. \quad (1)$$

This reaction converts the blue MB^+ to its colorless leuco form MBH, while glucose is oxidized to a gluconate-type species under alkaline conditions. In alkaline glucose solutions, this reduction can proceed repeatedly as long as both a reducing agent and hydroxide ions are available. The reduction pathway is generally considered slower than the oxidation step, which is consistent with the behavior required for the optical method (Anderson et al. 2012).

The oxidation of MBH back to MB^+ occurs when dissolved oxygen is present in the liquid:

$$O_{2(g)} \rightarrow O_{2(aq)}, \quad (2)$$

$$MBH + O_{2(aq)} \longrightarrow MB^+ + OH^-. \quad (3)$$

In contrast to the multi-step reduction pathway, the oxidation of MBH to MB^+ is a direct redox reaction and proceeds comparatively fast. Its effective rate is therefore governed primarily by the local availability of dissolved oxygen. Once oxygen reaches MBH at a location within the reactor, MBH is rapidly oxidized, and the liquid at that position returns to its characteristic blue color (Anderson et al. 2012; Piccione et al. 2017).

Taken together, the underlying redox cycle provides a chemically self-indicating system in which the visible color transition reflects the local rate of oxygen delivery to the liquid (oxygen supply). After the reactor has been driven into a uniformly reduced (colorless) state, any subsequent oxygen transported into the system is consumed locally to oxidize MBH. Although the reduction pathway remains active throughout the experiment, it proceeds substantially more slowly under the chosen alkaline glucose conditions. Consequently, the oxidation front is dominated by oxygen transport rather than by competing reduction, allowing the color change to serve as a reliable indicator of spatial oxygen supply (Anderson et al. 2012).

By monitoring the spatial pattern of reoxidation, two-dimensional fields of local oxygen supply times can be obtained. These fields directly reveal hydrodynamically induced oxygen-limiting zones and enable comparison of operating points or reactor configurations.

3 | Materials and Methods

All experiments were carried out in a double-impeller, laboratory-scale glass stirred tank reactor (STR) from Applikon (Figure 1). The total reactor volume is 3.2 L, while a filling volume of $V_{fill} = 2.7$ L was used during operation. The mixing system consisted of a Rushton turbine located at height $h_2 = d_2$ above the tank bottom and a three-bladed, down-pumping pitched-blade impeller positioned at $h_3 = 1.65 \times d_2$ above the Rushton turbine. The stirring speed was regulated and controlled by a HiTec Zang ViscoPakt-X7. Aeration was regulated

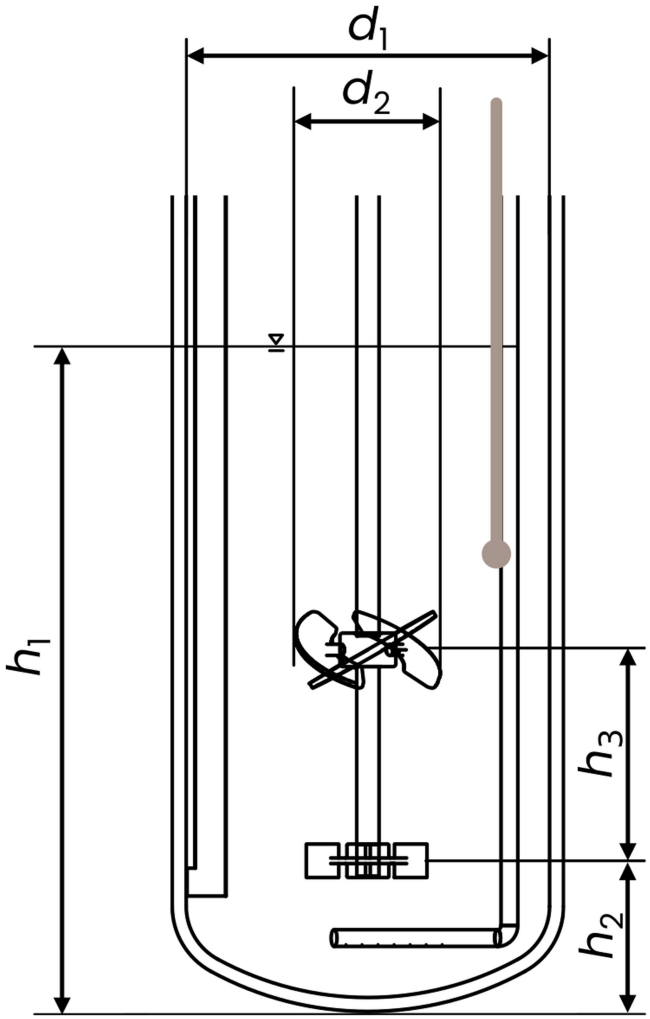

FIGURE 1 | Schematic of the stirred tank reactor used for the experiments.

by a Bronkhorst EL-Flow mass flow controller and introduced below the Rushton turbine through an eight-hole drilled sparger at a constant volumetric flow rate of $\dot{V}_G = 36\ \mathrm{Lh^{-1}}$. The STR was placed inside a temperature-controlled ($T \approx 21°C$) acrylic water bath filled with deionized water to minimize optical distortion during imaging.

Two categories of experiments were performed. First, the reaction-medium composition was systematically varied at constant aeration ($40\ \mathrm{Lh^{-1}}$) and constant impeller speed (160 rpm) in order to identify a stable and reproducible medium suitable for optical oxygen-supply measurements. Second, the selected medium was used to investigate hydrodynamic effects at impeller speeds of 0, 60, 160, 260, 360, and 460 rpm. The investigated agitation and aeration conditions were selected to represent a gentle aerated STR operating window relevant to mammalian-cell-type processes, rather than the higher gas-liquid throughput commonly used in microbial bioreactors.

The reaction medium consisted of deionized water, $V_{\mathrm{MBH}} = 2$ mL of a 1% aqueous solution of methylene blue, NaOH, and glucose. The density of the solution (1041.2 kg/m^3) was determined using a handheld Anton Paar DMA 35 density meter. To characterize the redox behavior of the system, NaOH concentrations of 0.100, 0.150, 0.175, 0.200, and 0.250 mol $\mathrm{L^{-1}}$ and glucose concentrations of 75, 100, 125, 150, and 175 g $\mathrm{L^{-1}}$ were tested. During these variations, when varying the glucose concentration, the NaOH concentration was kept constant at 0.200 mol $\mathrm{L^{-1}}$, whereas for variations in NaOH concentration, the glucose concentration was fixed at 100 g $\mathrm{L^{-1}}$. For each composition, the ability to establish the fully reduced colorless state during stripping with nitrogen and the reproducibility of the subsequent reoxidation behavior were evaluated. Only the global coloration time was considered during medium screening, while the DO signal was tracked to ensure constant, reproducible stripped and reoxygenated limits. Based on these results, a medium composition was selected that exhibited reliable reduction, clear oxygen-dependent colorization, and stable performance across operating points. The glucose concentration used in the reaction medium should therefore be understood as a reagent concentration required for the methylene-blue redox system, not as a representative substrate concentration of a production bioprocess. Similarly, the use of deionized water was chosen deliberately to establish a controlled model system and to isolate the influence of the reaction components on the optical response. Additional medium components present in real bioprocesses may influence the redox chemistry and therefore require separate evaluation in future studies.

Pure oxygen was used to establish a clearly directed and reproducible oxygen-driven colorization response. The increased oxygen availability accelerated the oxidation of MBH and reduced the risk that slow gas-liquid mass transfer or competing re-reduction of the indicator could obscure the spatial colorization pattern. The aim of this study was therefore not to reproduce the gas composition of a specific aerobic bioprocess, but to establish and evaluate the optical method under controlled and reproducible aerated STR conditions.

To measure dissolved oxygen, a needle-type optical DO probe (PreSens, Germany) was inserted through the STR head plate and positioned in the upper circulation loop, as schematically indicated in Figure 1 by the gray rod with the rounded tip. The probe was used in all experiments to monitor oxygen depletion during stripping with nitrogen, which was performed through a separate open-tube sparger regulated by its own Bronkhorst EL-Flow mass flow controller. After stripping, aeration with oxygen was only started once the STR had equilibrated under single-phase flow conditions.

The DO probe provides a local point measurement with its own sensor response time, whereas the optical evaluation represents a depth-integrated two-dimensional projection. Therefore, the two signals were not used for direct temporal correlation. The probe response time was not included in the determination of t_{col}, and all reported local and global colorization times were derived exclusively from the image-based methylene-blue analysis.

At the start of each experiment, the reaction media were driven into the fully reduced (colorless) state by stripping the oxygen with nitrogen. For this purpose, an open-tube sparger was temporarily inserted into the STR to ensure that only pure nitrogen passed through the vessel while the drilled-hole

sparger, its supply lines, and the mass-flow controller remained filled with only oxygen gas. Once complete reduction was verified visually and via the DO probe, nitrogen aeration was stopped, the open-tube sparger was removed, and the reactor was allowed to equilibrate for approximately 2 min under single-phase flow conditions. After this equilibration period, aeration with pure oxygen was initiated through the drilled-hole sparger. The onset of oxygen aeration defined $t = 0$ for both DO and optical measurements. Simultaneously, spatially resolved colorization was recorded using a Nikon D7500 camera positioned orthogonally to the reactor and illuminated from behind by a diffuse LED backlight panel. All recordings were performed with fixed optical settings (exposure time 1/1250 s, aperture f/8) to ensure consistency across experiments. The camera frame rate was set to 60 fps. Recording continued until the entire liquid volume had returned to the fully oxidized dark-blue state.

Image processing followed the pixel-wise evaluation strategy of Fitschen et al. originally developed for local mixing times. For each pixel (x, y), the gray-value trajectory $I(x, y, t)$ was normalized using its final oxidized value $I_\infty(x, y)$, yielding (Fitschen, Hofmann, Wutz et al. 2021)

$$\hat{I}(x, y, t) = \frac{I(x, y, t)}{I_\infty(x, y)}$$

The local colorization time $t_{col}(x, y)$ was defined as the earliest time at which $\hat{I}(x, y, t)$ exceeded 95% of I_∞. Where only bulk behavior was evaluated, the global coloration time was obtained as the point at which 95% of all pixels crossed the threshold. The resulting spatial maps represent two-dimensional fields of local oxygen-supply times within the reactor, enabling direct comparison of hydrodynamic conditions and operating regimes. It should be noted, however, that the optical measurement inherently represents a depth-integrated projection of the three-dimensional flow field. Consequently, local variations along the optical axis are superimposed in the recorded image, which may smooth spatial gradients and shift apparent colorization times compared to the true three-dimensional distribution. This limitation is inherent to the projection-based optical approach. However, the pixel-wise evaluation reduces systematic bias from spatially varying illumination, optical path length and local intensity differences, because each pixel is normalized with respect to its own final oxidized intensity and evaluated based on its own temporal gray-value development. Thus, pixels near the center shaft and pixels near the outer vessel region are not directly compared during the determination of $t_{col}(x, y)$. Instead, each projected pixel position is evaluated independently. The resulting fields should therefore be interpreted as a two-dimensional, indicator of local oxygen-supply dynamics rather than as a true planar cut through the reactor.

4 | Results

4.1 | Effect of Glucose Concentration on Redox Behavior

Before selecting a suitable reaction medium for the optical oxygen-supply method, it is necessary to evaluate whether variations in glucose concentration influence the oxidation behavior of the methylene-blue system. Glucose acts as the reducing agent that continuously regenerates the colorless leuco form (MBH), and therefore its concentration determines the overall "capacity" of the medium to undergo repeated reduction-oxidation cycles. In principle, insufficient glucose may slow or limit the reduction step, whereas excessive glucose could alter the balance between reduction and oxygen-driven oxidation.

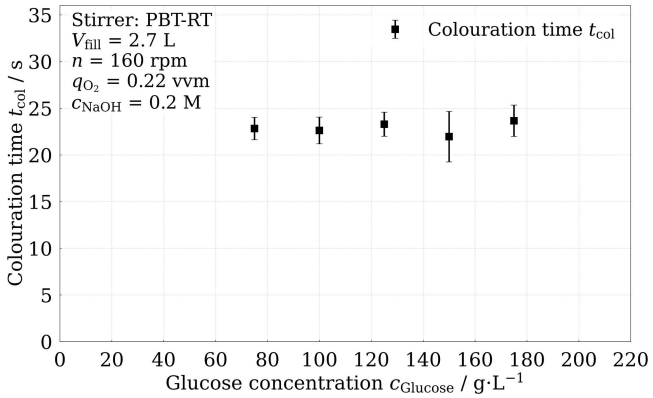

FIGURE 2 | Influence of glucose concentration on global colorization time in the range of 75–175 g · L^{-1}, data are shown as mean values from seven repeated experiments per operating point, with error bars indicating the standard deviation.

Figure 2 shows the experimentally determined global coloration time for glucose concentrations between 75 and 175 g L^{-1}. Across this range, once glucose is present in clear excess, further increases have no measurable influence on the global coloration time. All tested concentrations above approximately 75 g L^{-1} yield nearly identical global reoxygenation behavior, with colorization times consistently around 21–24 s. Each experimental operating point was repeated for a total of 7 times.

This agrees with the underlying reaction mechanism that under alkaline conditions the oxidation of MBH by dissolved oxygen is significantly faster than the concurrent reduction and is therefore transport-limited. Increasing the amount of glucose does not accelerate the oxidation step. Instead, it primarily extends the longevity of the medium by providing a larger pool of reducing equivalents. In practice, this means that higher glucose concentrations allow for more repeated color transitions before glucose becomes depleted, but they do not affect the time scale of the oxygen-driven colorization.

4.2 | Effect of NaOH Concentration on Redox Behavior

The NaOH concentration determines the extent of glucose enolization and thereby directly affects the rate of MB^+ reduction to its leuco form (MBH). Sufficient alkalinity is required to initiate the reduction step, but excessively high NaOH concentrations shift the chemical equilibrium strongly towards reduction. In these conditions, the medium may reduce MB^+ so rapidly and persistently that the oxygen-driven oxidation step cannot outcompete the reverse reaction. As a result, at very

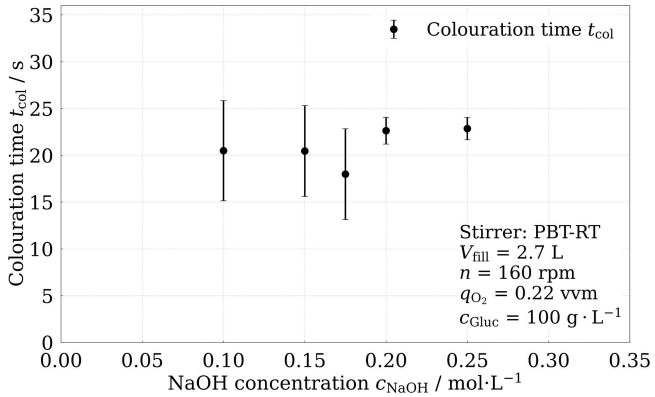

FIGURE 3 | Influence of NaOH concentration on global colorization time in the range of 0.10–0.25 mol L^{-1}, data are shown as mean values from five repeated experiments per operating point, with error bars indicating the standard deviation.

high NaOH levels, colorization may become extremely slow, unreliable, or may not occur at all under certain operating conditions. Consequently, the influence of NaOH concentration on the behavior of the indicator system is examined in the following.

Figure 3 shows the experimentally determined global coloration time for NaOH concentrations between 0.10 and 0.25 mol L^{-1}.

Two main trends emerge. First, the average global coloration time remains relatively constant across most of the tested range, with only modest systematic changes in the mean. This indicates that once NaOH is present at a sufficient concentration to enable rapid base-catalyzed enolization, the oxidation of MBH is again governed primarily by oxygen transport rather than by the reduction kinetics, consistent with both the chemical mechanism and the variation of glucose concentration results.

Second, the variability of the colorization time depends strongly on NaOH concentration. At lower NaOH levels (0.100–0.175 mol L^{-1}), reduction is slower and has a higher variability in the observed colorization behavior. Individual experiments at these concentrations show marginally faster reoxygenation colouration on average, but with large standard deviations. This reflects the sensitivity of the reduction reaction to local hydrodynamics when alkalinity is insufficient. Each experimental operating point was repeated for a total of 5 times.

At higher NaOH concentrations of 0.20–0.25 mol L^{-1}, the system becomes substantially more stable and reproducible. Here, the reduction step proceeds uniformly, but not so aggressively that it suppresses oxidation. The resulting colorization times are tightly distributed, and the medium maintains clear sensitivity to oxygen transport and allows for repeated cycles.

Above the upper end of the tested range of concentration, the medium becomes unusable as the reduction reaction becomes so dominant that the oxidation step through aeration and stirring does not occur until the reaction media becomes exhausted.

Overall, NaOH influences the stability and reliability of the colorization behavior more than the average colorization time itself. Low NaOH results in unstable behavior due to insufficient and heterogeneous enolization. Higher concentrations produce robust, oxygen-limited oxidation, while very high concentrations risk suppressing the oxidation step entirely.

This reinforces the importance of selecting a suitable window of NaOH concentration for the indicator system. For all subsequent experiments in this study, a NaOH concentration of 0.20 mol L^{-1} in combination with a glucose concentration of 175 g L^{-1} was chosen, as this operating point provided a stable, reproducible redox response without compromising the sensitivity of the oxidation step or reaching the solubility limit of glucose.

4.3 | Global Reduction Behavior Without Aeration

A central assumption underlying the optical oxygen-supply method is that the oxidation of MBH by dissolved oxygen proceeds on a much shorter timescale than the competing glucose-driven reduction to MB^+ under the selected reaction-medium conditions. To experimentally verify this assumption, additional experiments were conducted in which the reverse reaction was isolated. For this purpose, the oxygen supply was terminated after the medium had reached the fully oxidized state at the end of the forward reaction.

After completion of a standard colorization experiment, oxygen aeration was stopped, and the reactor was either left unstirred or stirred at the same impeller speed as during the preceding experiment, but without any further gas-liquid mass transfer. Under these conditions, the system returned from the oxidized blue state to the fully reduced, colorless state solely via the chemical reduction pathway. The time required for complete decolourization was evaluated using the same global 95% criterion applied for the colorization measurements.

These experiments were performed for the two extreme hydrodynamic operating points investigated in this study, namely 0 rpm and 460 rpm, using the selected reaction medium (0.20 M NaOH, 175 g L^{-1} glucose). Each condition was measured in triplicate to assess reproducibility.

At 0 rpm, the global decolourization time was $t_{red} = 1018 \pm 35$ s, corresponding to approximately 17 min. At 460 rpm, the reduction time was slightly shorter but of the same order of magnitude, with $t_{red} = 911 \pm 24$ s. The weak dependence on stirring speed indicates that, once oxygen aeration is stopped, the observed decolourization is governed primarily by the chemical reduction pathway rather than by hydrodynamic transport. The slightly shorter apparent reduction time at 460 rpm is attributed to enhanced single-phase mixing, which homogenizes the liquid phase and reduces local differences during decolourization. Residual oxygen transfer from the oxygen-containing headspace across the free surface may counteract reduction under single-phase stirring conditions. However, this effect is considered limited in the present setup because no self-aeration was observed and the upper impeller is sufficiently separated from the free surface.

These reduction times are more than one order of magnitude larger than the oxygen-driven colorization times observed under aerated conditions, which occur on the order of seconds for all investigated operating points. This comparison is not intended to provide a full kinetic characterization of the methylene-blue oxidation reaction or an explicit quantification of reaction-enhanced gas-liquid mass transfer. Instead, it is used to evaluate whether the competing glucose-driven reduction proceeds on a timescale that could obscure the oxygen-driven colorization response. Under the selected reaction-medium conditions, the reverse reduction pathway is sufficiently slow during the colorization experiments and does not dominate the measured local or global colorization times.

In gas-liquid reaction engineering, the coupling between reaction kinetics and mass transfer is commonly discussed using dimensionless quantities such as the Hatta number and the enhancement factor (van Krevelen and Hoftijzer 1947; Timmermann 2018). For oxygen-sensitive colorimetric systems, such analyses have been reported for the resazurin–dihydroresorufin system, where reaction-enhanced mass transfer was explicitly evaluated (Timmermann 2018; Reichmann et al. 2021; Xu et al. 2020). For the methylene-blue system used in the present work, corresponding kinetic parameters and Hatta-number data are, to the best of our knowledge, not available. Therefore, no explicit Hatta number is reported here. The colorization fields are instead interpreted as indicators of the combined effects of oxygen transport, gas-liquid mass transfer, and hydrodynamic redistribution under the investigated conditions. The conclusions drawn here therefore apply to the selected reaction medium of 0.20 mol L^{-1} NaOH and 175 g L^{-1} glucose, for which a clear separation between the slow reduction step and the faster oxygen-driven colorization response was experimentally confirmed.

4.4 | Spatial Characterization of Local Oxygen Supply

The methylene-blue method does not only yield a single global oxygen-supply time. It also provides full two-dimensional fields of local colorization time, $t_{col}(x, y)$, which reflect how rapidly dissolved oxygen reaches different regions of the vessel after the fully reduced state. These spatial fields offer a unique opportunity to visualize hydrodynamically induced heterogeneities in oxygen availability during reoxygenation, providing information that is not accessible through conventional point sensors. To ensure comparability between operating points, all experiments were conducted under identical chemical boundary conditions. Each run was first brought to a fully reduced, colorless state, and the dissolved oxygen concentration was verified to reach a reproducible low plateau. Only after equilibration under single-phase stirring, oxygen aeration was initiated, synchronizing the chemical and hydrodynamic starting conditions for all colorization experiments. The DO probe was used solely to verify reproducible oxygen-depleted and oxygen-saturated boundary conditions between operating points.

The overall trend in the global coloration time t_{col} is shown in Figure 4, which illustrates a monotonic decrease in colorization time with increasing impeller speed. This behavior reflects the expected enhancement in bulk oxygen transport under more turbulent conditions and visualizes a clear hydrodynamic dependence of the oxidation timescale. The systematic reduction in t_{col}, followed by diminishing sensitivity at higher agitation rates, confirms that the method responds to hydrodynamic intensification across the investigated operating range.

The observed trend is qualitatively consistent with behaviors reported for local mixing time measurements of aerated stirred tank reactors, where mixing times decrease with increasing agitation but tend to converge towards similar values at higher impeller speeds (Rosseburg 2019). The impeller Reynolds number was estimated according to

$$\mathrm{Re} = \frac{\rho_f \cdot n \cdot d_2^2}{\mu}, \tag{4}$$

using the measured liquid density $\rho_f = 1041.2$ kg/m^3, the impeller diameter $d_2 = 0.046$ m, the impeller speed n in s^{-1}, and the dynamic viscosity μ of the selected reaction medium. For the investigated reactor and operating conditions, Reynolds numbers exceeding approximately 10^4 provided only limited additional benefit in reducing global colorization time, consistent with observations from local mixing time studies. Furthermore, at higher agitation rates, the measured global colorization times remained on the order of tens of seconds and were therefore well above the temporal resolution of the optical acquisition at 60 fps.

Figure 5A–F presents representative local colorization time fields $t_{col}(x, y)$ for agitation rates between 0 and 460 rpm. At low agitation, the maps reveal large, slowly oxygenating regions with long t_{col}, consistent with weak macro-mixing and long supply times. Increasing agitation progressively shrinks these slow-oxygenation zones and produces more homogeneous and rapidly responding fields. Because the oxidation kinetics at the selected reaction-medium composition are sufficiently fast, spatial variations in t_{col} directly reflect variations in oxygen delivery rather than chemical artefacts. At higher agitation rates, where reoxygenation becomes more homogeneous and proceeds more rapidly overall, meaningful visualization requires a correspondingly narrower temporal scale.

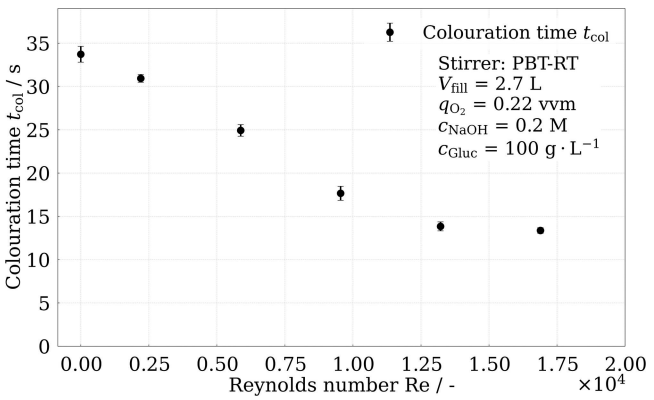

FIGURE 4 | Global colorization time t_{col} as a function of agitation speed, data are shown as mean values from 5 repeated experiments per operating point with error bars indicating the standard deviation.

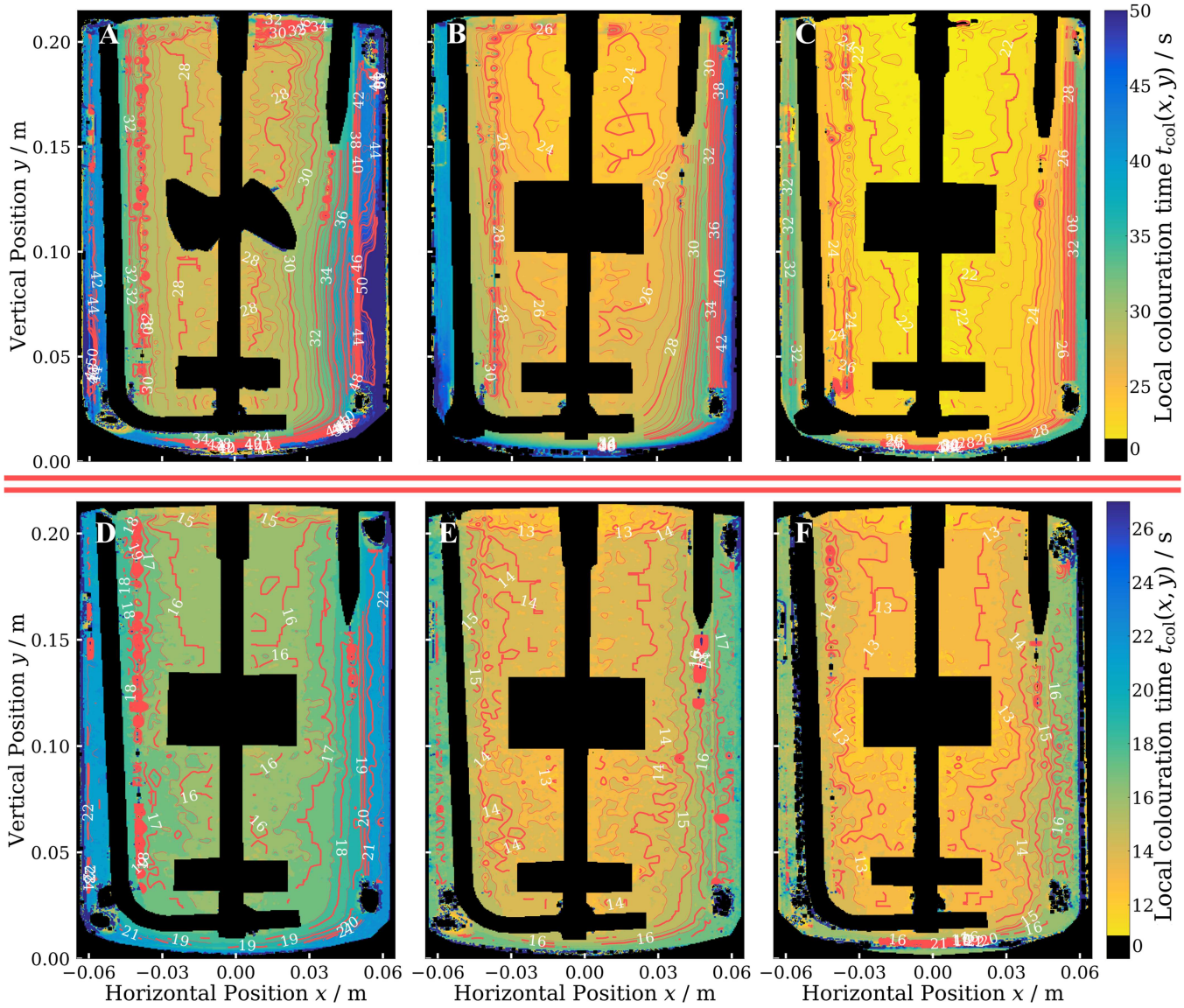

FIGURE 5 | Representative local colorization time fields $t_{col}(x, y)$ for agitation rates of A: 0 rpm, B: 60 rpm, C: 160 rpm, D: 260 rpm, E: 360 rpm, and F: 460 rpm. Subfigures A–C and D–F are displayed using separate color scales to preserve the visibility of spatial gradients at low and high agitation, respectively. The red horizontal divider visually separates the two color-scale groups, color values should therefore only be compared quantitatively within each row, not between rows.

Consequently, each colorization field is inherently operating-point specific, and gradients observed at one agitation rate are not directly transferable to another without accounting for these intrinsic differences in timescale. For visualization, subfigures A–C and D–F are displayed with two separate color scales, corresponding to the slower colorization at low agitation and the faster colorization at high agitation. The two rows are therefore separated visually in Figure 5, and color values should only be compared quantitatively within each row, not between rows.

The exemplary colorization fields in Figure 5 illustrate these trends across agitation rates A–F, particularly illustrated through the red contours. At 0 rpm (A), circulation is driven solely by the rising gas bubbles, leading to a narrow, fast-oxygenating plume above the sparger and extended regions of slow reoxygenation in the surrounding bulk. With a strong radial gradient originating from the central plume. At mild agitation (B), the impeller-induced circulation begins to redistribute the gas plume, reducing the extent of the slowly reoxygenating bulk region but still leaving pronounced slow oxygenating zones near the walls and in the lower corners indicated through the strong gradient, while the inter-impeller region benefits from the greater mass transfer boost from the impellers. At intermediate speeds (C,D), slow-oxygenation regions progressively diminish as the flow becomes more turbulent, indicating more uniform supply of dissolved oxygen. At the highest agitation rates (E,F), reoxygenation is rapid and nearly homogeneous across most of the liquid volume. The remaining gradients are concentrated mainly in the near-wall regions, where boundary-layer effects and weaker radial exchange limit local oxygen replenishment. This behavior demonstrates that, under strongly agitated conditions, the colorization fields primarily highlight residual transport limitations near solid boundaries rather than bulk oxygen-transfer constraints.

5 | Conclusion

This work introduces an optical method based on the reversible redox chemistry of methylene blue for visualizing and identifying local oxygen limitation in gas-liquid stirred tank bioreactors. By driving the reactor into a uniformly reduced state and monitoring the subsequent spatial reoxidation, the method provides two-dimensional fields of colorization times that reflect local oxygen supply governed by hydrodynamic transport and gas-liquid mass transfer.

The present experiments were conducted in deionized water to ensure well-defined and reproducible conditions. In real bioprocesses, additional factors such as medium composition, the presence of biomass introducing local transport resistances, and increased viscosity influencing mixing and gas dispersion may further affect oxygen transport. Consequently, the colorization times obtained in this study can be interpreted as a conservative estimate of oxygen-supply performance, such that regions identified as limited under these conditions are expected to be at least equally, if not more, critical in real bioprocess systems.

Systematic investigation of the reaction-medium composition demonstrated that glucose concentration primarily determines the longevity of the indicator system, while the NaOH concentration controls the stability and reproducibility of the redox response. Within a suitable operating window, the oxidation process remains dominated by oxygen availability rather than by chemical kinetics, enabling robust application of the method across a range of operating conditions.

Application of the method to a multiphase operated laboratory-scale stirred tank over a wide range of impeller speeds revealed characteristic spatial structures associated with oxygen-limiting regions. These include extended badly supplied zones under weak agitation, progressive homogenization with increasing turbulence, and residual transport limitations confined to wall-adjacent regions at high agitation rates. The observed patterns are consistent with known hydrodynamic features of stirred tanks and demonstrate that the method captures physically meaningful oxygen-supply heterogeneities.

In contrast to established local mixing time techniques based on tracer injection, the presented approach does not rely on a localized perturbation of the liquid phase. Depending on the injected volume, injection momentum, and density matching between tracer and bulk liquid, tracer addition can introduce an additional disturbance that may influence the measured mixing response. Oxygen aeration, in contrast, constitutes a normal operating condition in aerobic bioprocesses, with the colorization patterns emerging from the intrinsic interaction between hydrodynamics and gas-liquid mass transfer rather than from the initial distribution and subsequent homogenization of an injected tracer. As such, the method provides complementary information that is directly linked to oxygen availability rather than scalar homogenization alone.

Overall, the methylene-blue-based optical approach offers a simple, low-cost, and easily deployable tool for identifying oxygen-limiting operating points and spatial transport limitations in stirred tank bioreactors. Its ability to visualize oxygen supply coupled with the mixing conditions without intrusive sensing or tracer injection makes it particularly attractive for comparative studies, future scale-transfer investigations, and qualitative validation of CFD models of oxygen transport and gas-liquid mass transfer.

6 | Outlook

The presented optical method provides a simple means to visualize oxygen-supply heterogeneities under realistic aeration and mixing conditions. Future work should assess its applicability to more complex and process-relevant media and compare its spatial resolution and sensitivity to established laser-based oxygen-sensing techniques. In addition, systematic studies aimed at relating colorization times to local or bulk oxygen concentrations could further extend the method toward quantitative interpretation. Future developments could also combine the methylene-blue redox system with planar illumination, for example using a laser sheet or another defined light sheet, to reduce depth integration and obtain a more spatially resolved cross-sectional view. However, this would require a more specialized optical setup and would reduce the simplicity of the projection-based method presented here. The approach may also support CFD validation and the design of representative scale-down reactor concepts.

Author Contributions

Ryan Rautenbach: conceptualization, methodology, investigation, formal analysis, data curation, software, visualization, writing—original draft, review and editing. **Katharina Zörner:** investigation, methodology, writing—review and editing. **Jonas Barczyk:** writing—review and editing, discussion. **Marko Hoffmann:** project administration, supervision, writing—review and editing, discussion. **Ralf Takors:** funding acquisition, project administration, supervision, writing—review and editing, discussion. **Michael Schlüter:** funding acquisition, project administration, supervision, writing—review and editing, discussion.

Acknowledgments

This work was funded by the Deutsche Forschungsgemeinschaft (DFG, German Research Foundation) under grant number 427899833. Open Access funding enabled and organized by Projekt DEAL.

Conflicts of Interest

The authors declare no conflicts of interest.

Data Availability Statement

All data and post-processing scripts supporting the findings of this study are openly available in DaRUS at https://doi.org/10.18419/DARUS-5880, reference number 10.18419/DARUS-5880. The MATLAB code used in this study is based on the work of Fitschen, Hofmann, Wutz et al. (2021) and is available at Fitschen, Hofmann, Bernemann et al. (2021).

References

Anderson, L., S. M. Wittkopp, C. J. Painter, et al. 2012. "What Is Happening When the Blue Bottle Bleaches: An Investigation of the Methylene Blue-Catalyzed Air Oxidation of Glucose." *Journal of Chemical Education* 89, no. 11: 1425–1431. https://doi.org/10.1021/ed200511d.

Ascanio, G. 2015. "Mixing Time in Stirred Vessels: A Review of Experimental Techniques." *Chinese Journal of Chemical Engineering* 23: 1065–1076. https://doi.org/10.1016/J.CJCHE.2014.10.022.

Ascanio, G., M. Brito-Bazán, E. B.-D. L. Fuente, P. J. Carreau, and P. A. Tanguy. 2002. "Unconventional Configuration Studies to Improve Mixing Times in Stirred Tanks." *Canadian Journal of Chemical Engineering* 80: 558–565. https://doi.org/10.1002/CJCE.5450800419.

Bisgaard, J., M. Muldbak, S. Cornelissen, et al. 2020. "Flow-Following Sensor Devices: A Tool for Bridging Data and Model Predictions in Large-Scale Fermentations." *Computational and Structural Biotechnology Journal* 18: 2908–2919. https://doi.org/10.1016/j.csbj.2020.10.004.

Brooks, J. D., D. G. Maclennan, J. P. Barford, and R. J. Hall. 1982. "Design of Laboratory Continuous-Culture Equipment for Accurate Gaseous Metabolism Measurements." *Biotechnology and Bioengineering* 24, no. 4: 847–856. https://doi.org/10.1002/bit.260240408.

Cook, A. G., R. M. Tolliver, and J. E. Williams. 1994. "The Blue Bottle Experiment Revisited: How Blue? How Sweet?" *Journal of Chemical Education* 71, no. 2: 160. https://doi.org/10.1021/ed071p160.

Doran, P. M. 2013. Bioprocess Engineering Principles. Elsevier. https://doi.org/10.1016/B978-0-12-220851-5.00010-1.

Engerer, S. C., and A. G. Cook. 1999. "The Blue Bottle Reaction as a General Chemistry Experiment on Reaction Mechanisms." *Journal of Chemical Education* 76, no. 11: 1519. https://doi.org/10.1021/ed076p1519.

Fitschen, J., S. Hofmann, and V. Bernemann. 2021. "Gitlab Repository: Determination of Local Mixing Time Distribution in STR." https://collaborating.tuhh.de/v5/multiphase-bioreactors/sebastian-hofmann/determination-of-local-mixing-time-distribution-in-str.

Fitschen, J., S. Hofmann, J. Wutz, et al. 2021. "Novel Evaluation Method to Determine the Local Mixing Time Distribution in Stirred Tank Reactors." *Chemical Engineering Science: X* 10: 100098. https://doi.org/10.1016/j.cesx.2021.100098.

Gaugler, L., S. Hofmann, M. Schlüter, and R. Takors. 2024. "Mimicking CHO Large-Scale Effects in the Single Multicompartment Bioreactor: A New Approach to Access Scale-Up Behavior." *Biotechnology and Bioengineering* 121, no. 4: 1243–1255. https://doi.org/10.1002/bit.28647.

Gogate, P. R., and A. B. Pandit. 1999. "Survey of Measurement Techniques for Gas–Liquid Mass Transfer Coefficient in Bioreactors." *Biochemical Engineering Journal* 4, no. 1: 7–15. https://doi.org/10.1016/S1369-703X(99)00033-9.

Haringa, C., T. Tajsoleiman, W. A. van Winden, et al. 2025. "Flow-Following Sensor Technology, a Route to Validated cfd Models." *Biochemical Engineering Journal* 215: 109623. https://doi.org/10.1016/J.BEJ.2024.109623.

Hofmann, S., L. Buntkiel, and R. Rautenbach, et al. 2024. "Highlights Experimental Analysis of Lifelines in a 15,000 L Bioreactor by Means of Lagrangian Sensor Particles." *Chemical Engineering Research and Design* 205: 695–712.

Hofmann, S., R. Rautenbach, L. Buntkiel, et al. 2025. "Lagrangian Sensor Particles for Detecting Hydrodynamic Heterogeneities in Industrial Bioreactors: Experimental Analysis and Lattice-Boltzmann Simulations." *Chemical Engineering Journal Advances* 22: 100744. https://doi.org/10.1016/j.ceja.2025.100744.

Hoogendoorn, C. J. 1967. "Model Studies on Mixers in the Viscous Flow Region." *Chemical Engineering Science* 22: 1689–1699.

Kadic, E., and T. J. Heindel. 2014. *An Introduction to Bioreactor Hydrodynamics and Gas-Liquid Mass Transfer*. John Wiley & Sons. Google-Books-ID: IbYZAwAAQBAJ.

Kuschel, M., J. Fitschen, M. Hoffmann, A. VonKameke, M. Schlüter, and T. Wucherpfennig. 2021. "Validation of Novel Lattice Boltzmann Large Eddy Simulations (LB LES) for Equipment Characterization in Biopharma." *Processes* 9, no. 6: 950. https://doi.org/10.3390/pr9060950.

Kuschel, M., and R. Takors. 2020. "Simulated Oxygen and Glucose Gradients as a Prerequisite for Predicting Industrial Scale Performance a Priori." *Biotechnology and Bioengineering* 117, no. 9: 2760–2770. https://doi.org/10.1002/bit.27457.

Limpanuparb, T., C. Areekul, P. Montriwat, and U. Rajchakit. 2017. "Blue Bottle Experiment: Learning Chemistry Without Knowing the Chemicals." *Journal of Chemical Education* 94, no. 6: 730–737. https://doi.org/10.1021/acs.jchemed.6b00844.

Nienow, A. W. 1997. "On Impeller Circulation and Mixing Effectiveness in the Turbulent Flow Regime." *Chemical Engineering Science* 52: 2557–2565. https://doi.org/10.1016/S0009-2509(97)00072-9.

Nienow, A. W. 2014. "Stirring and Stirred-Tank Reactors." *Chemie Ingenieur Technik* 86, no. 12: 2063–2074. https://doi.org/10.1002/cite.201400087.

Piccione, P. M., A. A. Rasheed, A. Quarmby, and D. Dionisi. 2017. "Direct Visualization of Scale-Up Effects on the Mass Transfer Coefficient Through the "Blue Bottle" Reaction." *Journal of Chemical Education* 94, no. 6: 726–729. https://doi.org/10.1021/acs.jchemed.6b00633.

PreSens Precision Sensing GmbH. 2025. "Optical O2 Sensor Products." https://www.presens.de/products/o2.

Reichmann, F., J. Herath, L. Mensing, and N. Kockmann. 2021. "Gas-Liquid Mass Transfer Intensification for Bubble Generation and Breakup in Micronozzles." *Journal of Flow Chemistry* 11: 429–444. https://doi.org/10.1007/S41981-021-00180-3.

Rosseburg, A. 2019. "Influence of Heterogeneous Bubbly Flows on Mixing and Mass Transfer Performance in Stirred Tanks for Mammalian Cell Cultivation." PhD thesis, TUHH.

Rüttinger, S., C. Spille, M. Hoffmann, and M. Schlüter. 2018. "Laser-Induced Fluorescence in Multiphase Systems." *ChemBioEng Reviews* 5: 253–269. https://doi.org/10.1002/CBEN.201800005;REQUESTEDJOURNAL:JOURNAL:21969744;WGROUP:STRING:PUBLICATION.

Shuler, M. L., and F. Kargi. 2002. Bioprocess Engineering: Basic Concepts. Prentice Hall. 2nd ed. Prentice-Hall International Series in the Physical and Chemical Engineering Sciences.

Stine, J. M., L. A. Beardslee, R. M. Sathyam, W. E. Bentley, and R. Ghodssi. 2020. "Electrochemical Dissolved Oxygen Sensor-Integrated Platform for Wireless in Situ Bioprocess Monitoring." *Sensors and Actuators B: Chemical* 320: 128381. https://doi.org/10.1016/j.snb.2020.128381.

Tatterson, G. B. 1991. Fluid Mixing and Gas Dispersion in Agitated Tanks. McGraw-Hill.

Timmermann, J. 2018. "Experimental Analysis of Fast Reactions in Gas-Liquid Flows." PhD thesis, Hamburg University of Technology. http://hdl.handle.net/11420/5745.

van Krevelen, D. W., and P. J. Hoftijzer. 1947. "Studies of Gas Absorption. I. Liquid Film Resistance to Gas Absorption in Scrubbers." *Recueil des Travaux Chimiques des Pays-Bas* 66, no. 1: 49–65. https://doi.org/10.1002/recl.19470660106.

Van'tRiet, K. 1979. "Review of Measuring Methods and Results in Nonviscous Gas-Liquid Mass Transfer in Stirred Vessels." *Industrial & Engineering Chemistry Process Design and Development* 18, no. 3: 357–364. https://doi.org/10.1021/i260071a001.

Weiland, C., E. Steuwe, J. Fitschen, et al. 2023. "Computational Study of Three-Dimensional Lagrangian Transport and Mixing in a Stirred Tank Reactor." *Chemical Engineering Journal Advances* 14: 100448. https://doi.org/10.1016/J.CEJA.2023.100448.

Wolfbeis, O. S. 2015. "Luminescent Sensing and Imaging of Oxygen: Fierce Competition to the Clark Electrode." *BioEssays* 37, no. 8: 921–928. https://doi.org/10.1002/bies.201500002.

Xu, F., G. Hébrard, and N. Dietrich. 2020. "Comparison of Three Different Techniques for Gas-Liquid Mass Transfer Visualization."

International Journal of Heat and Mass Transfer 150: 119261. https://doi.org/10.1016/j.ijheatmasstransfer.2019.119261.

Zhang, Y., H. Yang, W. Gao, and C. Wu. 2024. "Research Progress of Optical Dissolved Oxygen Sensors: A Review." *IEEE Sensors Journal* 24, no. 19: 29564–29574. https://doi.org/10.1109/JSEN.2024.3441692.

Zlokarnik, M. 1999. R¨uhrtechnik Theorie und Praxis. Springer. https://d-nb.info/954872479/04. Verfahrenstechnik. OCLC: 263984718, accessed 2025- 04-16.